

# INVESTIGATING (RE)-ENTRIES FROM SPACE: IN-SITU AND REMOTE MEASUREMENTS WITH THE CUBESAT SOURCE

J. Petri<sup>(1)</sup>, D. Galla<sup>(1)</sup>, P. Hoffmann<sup>(2)</sup>, K. Gebhard<sup>(2)</sup>, L. Blümmler<sup>(2)</sup>, and S. Klinkner<sup>(3)</sup>

<sup>(1)</sup>*Institute of Space Systems, University of Stuttgart, Germany, Email: petri@irs.uni-stuttgart.de*

<sup>(2)</sup>*Small Satellite Student Society at the University of Stuttgart (KSat e.V.)*

<sup>(3)</sup>*Institute of Space Systems, University of Stuttgart, Germany, Email: klinkner@irs.uni-stuttgart.de*

## ABSTRACT

The *Stuttgart Operated University Research Cubesat for Evaluation and Education (SOURCE)* is currently being developed University of Stuttgart's Institute of Space Systems and the Small Satellite Student Society at the University of Stuttgart (KSat e.V.). The project is currently in Phase D, the launch is planned for end of 2023. The main scientific mission objectives are dedicated to the remote observation of meteors and in-situ measurements of the satellite re-entry.

Regarding the in-situ re-entry measurements, the satellite is equipped with multiple sensors to measure the heat-flux, temperature and pressure during re-entry at the end of the mission. Those measurements shall be compared to simulations and experimental data of plasma wind tunnel experiments, which are conducted at the Institute of Space Systems (IRS) as well. The different measurements and simulations complement each other in order to understand the re-entry process and improve existing break up models. As a result, future satellites can be designed to completely disintegrate during re-entry and avoid space debris.

Additionally, oxygen sensors are used to measure the concentration of atomic and molecular oxygen at different altitudes. This paper describes the sensor setup and test as well as the expected scientific output and current status of the development.

The remote measurements are dedicated to the observation of meteors. These observations are used to determine the meteoroid flux and improve existing meteoroid mass models. Thus, future satellites can be designed to cope with the expected meteoroid flux. This helps to avoid space debris caused by unexpected hits from meteoroids, which lately happened to the James Webb telescope. The meteor observation is done by pointing a visual camera towards Earth and continuously taking images during Eclipse. Since it is not possible to downlink all images, an on-board detection algorithm is necessary and mission critical. The *SOURCE* satellite is used to qualify the instrument, demonstrate the feasibility of space based meteor observation and test the detection algorithm. In

this paper the current status of the instrument development as well as the observation concept taking into account constraints from the satellite bus and the expected scientific output are given. *SOURCE* is a unique mission combining remote and in-situ measurements dedicated to (re-)entry observations. This paper gives an overview of the scientific goals, the instrumentation and current status of the development. Furthermore, the expected scientific output is given.

Keywords: Debris, re-entries, meteor observation.

## ACRONYMS

ArtMESS Artificial Meteorvideo Simulation Software; CotS Commercial of the Shelf; EPS Electrical power supply; ESA European Space Agency; FIPEX Flux Phi Probe Experiment; FM Flight Model; FOV Field of View; FSFW Flight Software Framework; GPS Global Positioning System; HEFDiG High Enthalpy Flows Diagnostics Group; IAG Institute of Aerodynamics and Gas Dynamics; IRS Institute of Space Systems; KSat e.V. Small Satellite Student Society at the University of Stuttgart; MeSHCam Meteor observation, Star and Horizon tracking Camera; OBC On Board Computer; PCB Printed Circuit Board; PLOC Payload On-Board Computer; PRIma PR Imager; QM Qualification Model; SoC State of Charge; *SOURCE* Stuttgart Operated University Research Cubesat for Evaluation and Education; SpaceMEDAL Spaceborne METEOR Detection ALgorithm; SSO Sun-synchronous Orbit; SWARMS Simulator for Wide Area Recording of Meteors from Space; SWARMSv2 SWARMS Version 2; US University of Stuttgart; USLP Unified Space Data Link Protocol

# 1. INTRODUCTION: MISSION OBJECTIVE AND DESCRIPTION

*Stuttgart Operated University Research Cubesat for Evaluation and Education (SOURCE)* is a CubeSat mission developed by the at the University of Stuttgart (US)'s Institute of Space Systems (IRS) and the Small Satellite Student Society at the University of Stuttgart (KSat e.V.). The project is conducted by students and coordinated by employees and PhD students from the University of Stuttgart. Similar, the subsystems of the satellite are developed by students under the supervision of at least one PhD student. Since 2020 *SOURCE* is part of the European Space Agency (ESA) *Fly your satellite program!* program, which is giving access to facilities and support from ESA experts as well as financing the launch. The project is currently in Phase D, the launch is planned for 2023/2024. A rendering of the 3+ unit CubeSat is shown in Figure 1.

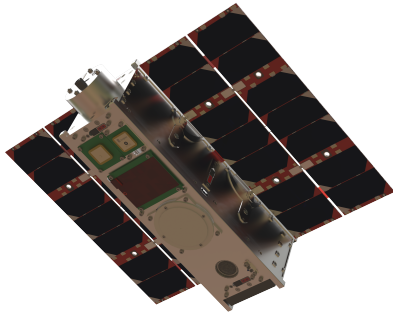


Figure 1. CAD drawing of the SOURCE satellite with both solar panels already deployed.

The mission data is summarized in Table 1.

Table 1. SOURCE mission facts

Property	Value
Orbit	Sun-synchronous/ ISS orbit
Orbit altitude	450 km to 500 km
Mass	~ 5 kg
Size	30 cm × 10 cm × 10 cm
Mission duration	~ 1 year
Attitude determination	Sun sensors, magnetometer, experimental Startracker
Attitude control	Magnetorquer
Pointing accuracy	5°
Position determination	Global Positioning System
Max. power generation	30 W
Payload data rate per day	100 MB using S-band

The project gives students the opportunity to work on a satellite project and gain technical and procedural experience. Furthermore, a satellite platform for future missions should be developed. Finally, the satellite serves

as a platform for technology demonstration. The primary and secondary mission objectives are outlined in Table 2.

Table 2. SOURCE mission objectives

Primary objectives	
O 1.1	<i>Education</i> - To provide university students with the opportunity to gain technical and procedural experience in all mission phases of a satellite system.
O 1.2	<i>CubeSat platform</i> - To design and validate a reproducible CubeSat platform for a small satellite educational program.
O 1.3	<i>Technology verification</i> - To verify different platform technologies for further mission in the small satellite educational program.
Secondary objective	
O 2.1	<i>Demise investigation</i> - To investigate interactions between entry objects and the outer atmosphere.

In this paper the scientific goals and expected outcome of the demise investigation objective shall be given.

## 1.1. Scientific background of the SOURCE mission

The demise investigation objective is separated into two main scientific goals:

First, the mission shall perform atmospheric and re-entry science using a sensor suite. This sensor suite should perform measurements below an altitude of 200 km in order to verify the simulation software PICLas (developed by University of Stuttgart's Institute of Space Systems and Institute of Aerodynamics and Gas Dynamics (IAG), see [1]). PICLas is a flexible particle-based plasma simulation suite for the numerical simulation and modelling of re-entry flow. Additionally, the sensors suite includes two Flux Phi Probe Experiment (FIPEX) sensors to measure atomic oxygen, pressure sensors as well as two kinds of heat flux and temperature sensors. During the re-entry of *SOURCE*, these sensors deliver data about the atmosphere, which is downlinked using the satellite network Iridium. Using this network is necessary, since the re-entry is short and most likely not over a ground station.

Second, a monochromatic camera called Meteor observation, Star and Horizon tracking Camera (MeSHCam) is used to observe meteors during the satellite eclipse. The camera is pointed towards the Earth and is continuously taking images. Due to the limited downlink capacity, a meteor detection algorithm called *Spaceborne METeor Detection ALgorithm (SpaceMEDAL)* is developed and used to detect images containing a meteor and downlinking only these images. The data about meteors is used to determine the meteoroid flux to improve existing meteoroid mass models. Those models are crucial

for planning safe space activities such as astronauts extra-vehicular activities or satellite missions. For example, recently the new James Webb telescope was hit by an unexpectedly large meteoroid (see [2]). While the telescope still fulfils all requirements, this incident underlines the importance of understanding the meteoroid environment for space missions.

To sum up, the scientific mission of *SOURCE* is a contribution to the surveillance of space debris and improvement of meteoroid models in order to access risk for satellites as well as a contribution to improve re-entry models in order to improve simulations. In the following, details about the sensors suite and meteor observation instrument are given, the scientific background is outlined and the expected scientific output is analysed.

## 2. IN-SITU MEASUREMENTS

The in-situ measurement suit for *SOURCE* can be divided into a re-entry and an atmospheric focused part. To analyse the demise of the satellite, heat flux, temperature and pressure sensors are combined in five sensor arrays, each consisting of a set of the utilized sensors, in different locations on the surface of *SOURCE*. For the atmospheric science, two FIPEX sensors are located in the front and back of the satellite body. The placement of the in-situ measurement sensors was defined with a six-degrees-of-freedom simulation of *SOURCE* during the early phase of re-entry. Figure 2 displays the allocation of the in-situ sensors and gives an insight of the idea of placement. With an expected satellite tumbling frequency of around  $5^\circ/\text{s}$ , the re-entry sensor are distributed on linearly independent sides to investigate the heat flux for different angles of attack with the possibility of gradient measurements with 2 arrays on the same side at the bottom. FIPEX sensors are placed in the front and back to measure stagnation point and wake concentration of atomic oxygen. The respective in-situ measurement sensors are discussed in detail below.

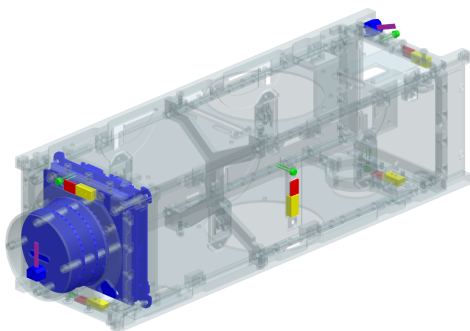


Figure 2. Placement of sensors on *SOURCE*. Pressure (green), commercial heat flux (red), IRS heat flux (yellow) and FIPEX (magenta) sensors as well as the dedicated circuit boards (blue) are highlighted.

## 2.1. Re-entry sensors

The purpose of the re-entry sensors is to obtain in-situ data of the early phase of *SOURCE* demise in an altitude of 200 km to 130 km. These measurements should be used for a software validation and improvement for re-entry forecast simulations to increase the understanding of the demise process of satellites and other structures from orbit. These re-entry analysis should define the ground impact risk of space debris and help mitigate it by adapted space craft design. A combination with plasma wind tunnel experiments is currently developed [3] *SOURCE* utilizes three different sensors for the data acquisition which are discussed below.

### 2.1.1. Re-entry sensor overview

The three different types of sensors for early phase re-entry measurements for each of the five sensor arrays on the satellite collect data of temperature, pressure and heat flux on the satellite's surface. Figure 3 illustrates their assembly. For the heat flux measurements, two approaches on different sensors are utilized with one being commercially available and the other one an in-house development. The read-out is done with a Vorago VA10820 micro controller, which is connected via RS485 to the On Board Computer (OBC) of *SOURCE*. For the selection process of the re-entry sensors, several PIClas simulations were conducted with preliminary atmospheric and orbital data [4].

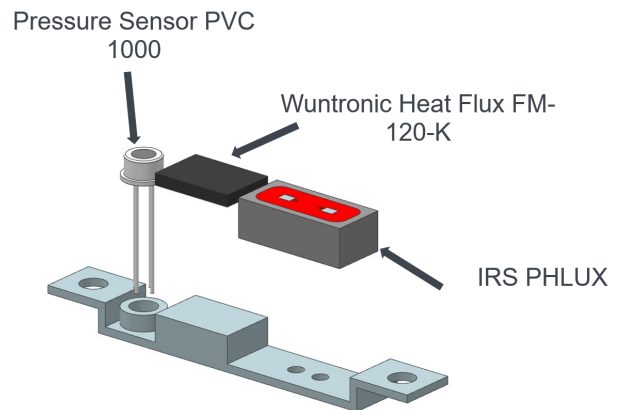


Figure 3. Setup of one of the five re-entry sensor arrays.

### 2.1.2. Pressure sensors

Pressure measurements will be conducted with PVC 1000 sensors from POSiFA Microsystems Inc. These micro Pirani gauges measure changes in resistance of a heated element caused by heat transfer to surrounding particles. The thermal conductivity is proportional to pressure in the low vacuum range, hence this correlation can determine the pressure with a low response time. In

the satellite, the sensor is supplied with a constant current source so that a change in resistance leads to a change in voltage, which is converted to a digital number and monitored by the payload micro controller. The achieved resolution will be around 0.6 Pa with a range of 0.1 Pa to 4000 Pa. Even though this accuracy is not ideal for the expected pressure range during early phase of re-entry, these sensors were a trade-off selection due to their simplicity and size.

### 2.1.3. Heat flux and temperature sensors

The commercial heat flux and temperature sensors are FM-120-K from Wuntronic. They consist of a thermocouple and a thermopile with a discrete read-out. The thermocouple utilizes the Seebeck effect to generate a temperature-dependent voltage via contact of two different electrical conductors. For the thermopiles, which are several thermocouples connected, the heat flux can be calculated from the temperature difference of the top and bottom side of the sensors with a known conductivity coefficient. The measured heat flux range is from  $-3300 \text{ W/m}^2$  to  $6800 \text{ W/m}^2$  with a resolution of  $300 \text{ mW/m}^2$ .

### 2.1.4. Phlux sensors

To investigate the incoming heat flux from surface recombination effects during re-entry, an in-house developed PHLUX sensor is also flown onboard *SOURCE* [5]. This PHLUX sensor consist of of two PT1000 with different coating. The measurement principle is based on the different recombination rates of atomic oxygen on two surfaces with known, dissimilar catalytic properties. Predetermined and qualified models based on a low thermal conduction from the sensor to the mounting are then used to derive the incoming heat flux form the measured temperature. The measurement can then be used to determine the impact of recombination rates on the heat flux of the satellite's surface.

### 2.1.5. Hardware implementation

All re-entry sensor arrays are connected to two Printed Circuit Boards (PCBs) in the front of the satellite, where analogue signals are amplified and digitalized (see Figure 4). These PCBs are in-house developed and consist of 4 layers each. The frequency of the sensor-read outs are controlled by the Vorago micro controller on them, which also is responsible for data compression and storage. Several versions of these re-entry PCB boards were already successfully tested in a thermal vacuum chamber and the newest iteration will be qualified on a shaker [6].

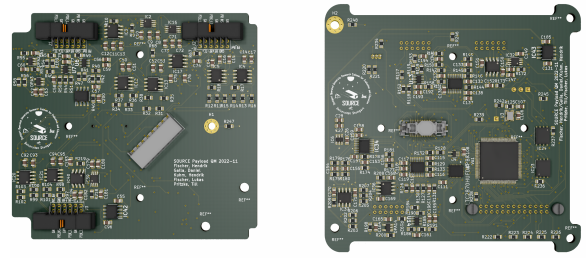


Figure 4. Rendering showing the front side of the QM3 model of the two sensor payload PCBs.

### 2.1.6. Sensor calibration

The next milestones for the re-entry sensors will be a detailed calibration for expected values during early phase of *SOURCE*'s demise. These include tests of the pressure sensor in very low vacuum environment with a high accuracy calibration device. Moreover, heat flux sensors will be calibrated with a laser setup to induce a defined flux. The before mentioned plasma wind tunnel tests will enable a test of the sensor setup in a very similar plasma environment, hence enabling an insight into the Phlux respond to recombination effects.

## 2.2. FIPEX

FIPEX are lightweight, small-scale oxygen sensors with low power consumption, which makes them ideally suited for satellite applications. They are currently developed by the High Enthalpy Flows Diagnostics Group (HEFDiG) at the University of Stuttgart.

Two FIPEX sensors equipped with platinum pickup electrodes are mounted on the *SOURCE* CubeSat, one at the nose and one at the rear (see Figure 2). The electronics necessary to regulate the sensors are housed in the cylindrical structure extension in the nose of the satellite, also called the "Tuna Can". They consist of three PCBs designed by the electrical workshop at the University of Stuttgart's Institute of Space Systems. Two boards are equipped with inverters and relays, one board for each sensor to provide power. The third board is the controller board equipped with a micro controller used to control and communicate with the sensors.

FIPEX sensors have thus far flown on sounding rockets and gathered data up to an altitude of 110 km [7][8]. On *SOURCE*, they shall gather data starting from the expected initial altitude of 300 km to 400 km down to 200 km where the satellite is expected to begin its demise. In contrast to the operation on sounding rockets, *SOURCE* as an orbital platform allows for longer measurements, which were initially designed to last 120 s. However, due to oxygen build up on the sensing electrodes during orbit, the measurements are now aimed to last 5 min to 10 min. This allows the banked up oxygen to dissipate during the first minutes of the measurement

before the sensor signal can be trusted to reflect the current oxygen flux. The duration of the measurements will be limited by the power budget of the satellite.

FIPEX sensors consist of two sides, one containing the pickup electrodes and the opposing side containing the heating circuit made from platinum [9] as represented in Figure 5. The sensors mounted on *SOURCE* feature platinum pickup electrodes and will therefore be measuring atomic oxygen concentrations. Other versions of the FIPEX sensor feature gold electrodes, which can be used to determine molecular oxygen levels but will not be part of the *SOURCE* mission. Sensor and heater are housed in the head of the sensor. They are separated by a solid electrolyte layer spread over a substrate. The solid electrolyte becomes conductive for oxygen anions at a certain temperature. Thus, the sensor current created by the oxygen flux originating from the approaching flow can be measured.

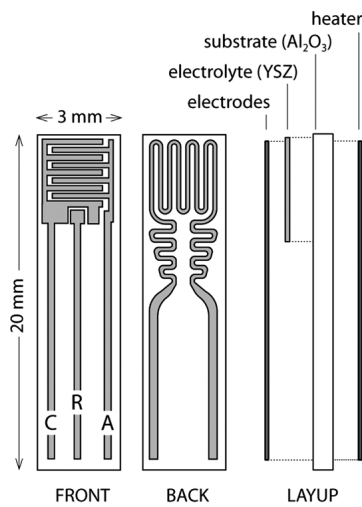


Figure 5. Schematic layout of FIPEX oxygen sensor. Front: Sensing Cathode (C) and Anode (A) with reference electrode. Back: Platinum resistance heater.

The core of the control electronics of the FIPEX system on *SOURCE* is a PIC24 micro-controller. It receives commands to heat-up or power-down the sensors individually from the OBC and returns sensor data upon request. The micro-controller runs a synchronous control loop that adjusts the voltage of the heater of each individual sensor in order to obtain the correct resistance value as set by the OBC. The heater's resistance is determined as the quotient of heater voltage and heater current measured during each iteration of the loop.

Accuracy of FIPEX measurements on *SOURCE* is determined by the sensor's own tolerances but also positional data and attitude knowledge from the satellite. Velocity and angle of the oncoming flow are essential for the accurate interpretation of the FIPEX data to model the oxygen flux correctly [10]. During normal orbital conditions, attitude control of *SOURCE* consisting of magnetorquers allow for an accuracy of  $5^\circ$ . Below an altitude of 200 km, attitude control and knowledge can no longer

be guaranteed as tumbling forces become too great. As such, *SOURCE* is expected to record qualitative data during the final phases of re-entry.

As of the current development Phase D of the *SOURCE* CubeSat, FIPEX has already undergone and successfully completed extensive testing. All functionality of the system could be verified under laboratory and thermal-vacuum conditions. RS485 communication was successfully tested using an Arduino to simulate an OBC.

The FIPEX system underwent two thermal-vacuum tests successfully in 2022, which were conducted in the thermal-vacuum-chamber of the University of Stuttgart. During these tests, power consumption was determined at 7 W or less depending on the environmental temperature for a sustained measurement. However, during heat-up, a big spike in power consumption was evident, which prompted the adjustment of the control loop, increasing the heat-up time but decreasing the spike in power consumption. In the thermal-cycle test, FIPEX could successfully be verified for a non-operational temperature range of  $-35^\circ\text{C}$  to  $80^\circ\text{C}$  in 1 cycle and an operational temperature range of  $-19^\circ\text{C}$  to  $74^\circ\text{C}$  over a total of 8 cycles.

As its current status, FIPEX on *SOURCE* has completed subsystem-level hardware qualification with its Qualification Model (QM). Furthermore, the production of the Flight Model (FM) is finished. In terms of software, the PIC24 now requires implementation of *SOURCE*'s Unified Space Data Link Protocol (USLP) for communication with the OBC. This constitutes the last integration step of the system and will make way for a full functional test with the OBC module on a Flatsat assembly. The sensor FMs will be calibrated in the high-vacuum oxygen flow chamber from the HEFDiG group (see [10]) as close as possible to the launch date to ensure the best accuracy possible.

A challenge arising from the unprecedented operation of the sensors in orbit as compared to operation on sounding rockets is the possible demise of the solid electrode layer. As FIPEX sensors have never served on a comparable long-term mission, their performance over time will be investigated during the mission. Lastly, the exact time for each measurement will need to be determined. While from a scientific standpoint, longer measurements of i.e. 10 min would be desirable, the length of each measurement is primarily limited by the power budget of the satellite. To enable more measurements during each orbit (for example at multiple points of interest), a shorter measurement time may therefore be chosen.

### 3. REMOTE MEASUREMENTS

In addition to the in-situ measurements, the *SOURCE* satellite will carry out remote measurements beforehand. For this purpose, a camera system is integrated in the

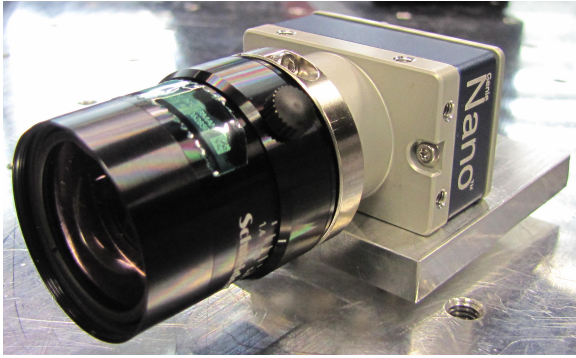


Figure 6. MeSHCam in the optical laboratory: The camera GenieNano M1920 equipped with a Schneider Kreuznach Cinegon 1.4/12.

satellite. It consists of two cameras oriented perpendicular to each other. One camera is used for Earth observation (called PR Imager (PRIma) and will not be discussed in this paper. The second camera's main task is meteor observation. Additionally, the camera serves as a technology demonstration as it can be used for star and horizon tracking to determine the satellite's attitude. Due to its tasks, the camera combined with its lens is referred to as Meteor observation, Star and Horizon tracking Camera (MeSHCam). The components can be seen in Figure 6.

The task focused on in this paper is the meteor observation. For clarification, Figure 7 distinguishes between meteors, meteoroids and meteorites. The MeSHCam will be used to determine the meteoroid flux by observing meteors caused by meteoroids when they enter Earth's atmosphere. With the instrument setup it is therefore possible to improve mass models. Consequently, *SOURCE* demonstrates the feasibility and performance of commercial off the shelf components that are not designed for the use in space in particular.

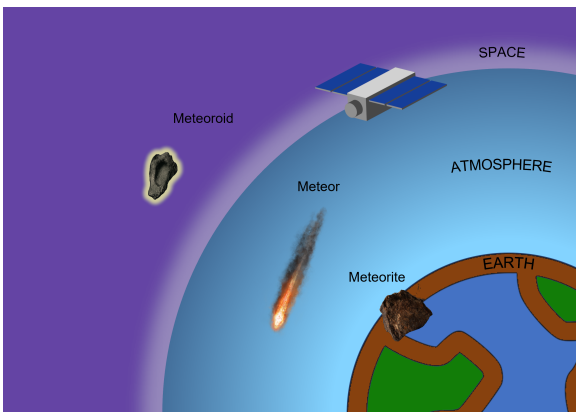


Figure 7. Difference between meteoroid, meteor and meteorite.

### 3.0.1. Observation concept

The meteor observation is done during eclipse with the satellite in nadir pointing mode. In this mode MeSHCam will point towards the Earth, the optical axis exactly aligned with the direction of gravity. The instrument is continuously taking images, meteors will appear as bright pixels in the camera image. In order to prevent Earth's rotation and *SOURCE*'s movement from blurring the images, a short exposure time is chosen. Furthermore, evaluating the sequence of images allows to measure the speed of meteors. This detection technique results in huge amounts of image data in very short timeframes: 30 min of observation create 4 GB of data. Because *SOURCE* is only able to downlink around 100 MB/day, an on-board detection algorithm is necessary to identify images containing a meteor. In the acquired images other light sources are visible as well such as cities, lightning flashes, and airplanes which makes filtering the images for meteors challenging. After the processing only the images containing meteors will be linked down. A designated processing unit is integrated in *SOURCE* to run the algorithm called Payload On-Board Computer (PLOC).

### 3.0.2. The instrument

The chosen camera *GenieNano M1920* is a commercial off the shelf (COTS) unit. It features large pixels with a high quantum efficiency while being light-weight and small enough to fit on the CubeSat platform. The 2.3 MP resolution results in a decent image quality while keeping the needed data storage space down. A Gigabit Ethernet interface is used to transfer images to the PLOC and command MeSHCam.

The *GenieNano M1920* requires a C-mount lens with a small f-number to ensure that even with short exposure times enough light can be captured by the camera sensor. The lens *Schneider Kreuznach Cinegon 1.4/12* fulfils both criteria. Additionally, it has a small aperture of 1.4 and the focal length of 12.7 mm results in a Field of View (FOV) of  $48^\circ \times 31^\circ$ .

To process the images with an algorithm, the *Trenz TE0720* is used as the PLOC. Because the payload is not mission critical, a unit with decent processing power can be used instead of a less powerful but radiation hardened device. The *Trenz TE0720* holds the Zynq XC7Z020 FPGA processor containing 1 GB of DDR3 RAM. A 32 GB SD-card is used as a hard drive to hold the operating system, necessary programs and store image data. The algorithm and camera control software depend on OpenCV and CVB CameraSuite which are available on Linux. For that reason, Ubuntu was chosen as an operating system. The algorithm to detect meteors in the images is being developed at the University of Stuttgart (see [11]). The most important characteristics of the instrument components are summarized in table Table 3.

Table 3. MeSHCam characteristics and properties

<i>Trenz TE0720</i>	
Processor	Xilinx Zynq XC7Z020
RAM	1 GB DDR3
Memory card size	32 GB
OS	Ubuntu 18.04 LTS
PHY interfaces	SPI, I <sup>2</sup> C, USB, Gigabit Ethernet
Mass	47.8 g
<i>GenieNano M1920</i>	
Sensor type	CMOS
Resolution	1920 px × 1200 px (2.3 MP)
Pixel size	5.86 μm × 5.86 μm
Quantum efficiency	86 % at 528 nm
Mass	46 g
Dimensions	44 mm × 26 mm × 40.6 mm
Voltage	12 V
Power consumption	2.82 W
<i>Schneider Kreuznach Cinegon 1.4/12</i>	
Focal length	12.7 mm
F-number	1.4
FOV	48° × 31°
Mass	89 g

### 3.0.3. Testing facilities

The camera system is a technology demonstration of commercial off the shelf components. Therefore, none of the integrated components are designed for the use in space. Following that, comprehensive tests are needed for all components. All optical tests are performed in an optical section in an ISO 8 clean room at the University of Stuttgart. These tests include EMVA1288 tests as well as camera characterisation and algorithm calibration tests. The room can be darkened completely with black curtains. A testbed for camera operations is also present, which consists of an LG OLED55B8LLA television screen surrounded by additional black curtains to further improve darkness on camera tests. On the screen, geometric calibration targets or videos with artificial meteors can be shown. For a detailed description of the artificial meteor generation, please refer to [12]. In front of the television screen, an optical rail is positioned perpendicular to the screen. It can be used to align the components. A setup containing both cameras and the PLOC in the testbed can be seen in figure Figure 8.

The environment tests of the system are comprised of thermal vacuum tests and a shaker test. 8 cycles reaching from  $-20^{\circ}\text{C}$  to  $60^{\circ}\text{C}$  were performed under the pressure of  $3 \times 10^{-5}$  mbar. The shaker test will be performed at the ESA ESTEC facility in Noordwijk. The tests ensure that all components are physically suited for their use in space.



Figure 8. Testbed in the optical section of the cleanroom at the University of Stuttgart's Institute of Space Systems.

## 3.1. Expected scientific output

Since the scientific objective is the determination of the meteoroid flux, a large number of meteors should be observed in order to get solid statistic data. Thus, in the following the scientific output is defined as the number of meteors detected with MeSHCam. The expected scientific output of the MeSHCam instrument depends on the instrument itself as well as constrains from the satellite bus which are outlined in the following.

### 3.1.1. Methodology and constrains

In order to determine the number of detected meteors, first the detection rate must be determined depending on instrument parameters and mission characteristic. Then, the detection rate can be determined taking into account satellite bus constrains.

**Limiting magnitude and detection rates** Regarding the instrument parameters influence on the scientific output, the limiting magnitude of the instrument is considered. This limiting magnitude describes which brightness meteors need to have in order to be observed by the instrument. Since the number of meteors increases logarithmic with decreasing brightness, a higher limiting magnitude is desirable to observe more meteors.

The limiting magnitude depends on several factors, e. g. instrument parameters like sensor (e. g. pixel size, quantum efficiency) and lens (e. g. aperture size) properties as well as meteor properties (e. g. velocity) and mission parameters (e. g. orbit altitude). A simulation has been developed, to calculate the limiting magnitude for a typical meteor occurring in the centre of the sensor moving across the sensor. See [13] for more details on the simulation. While the simulation has some limitations, the calculated limiting magnitude is accurate enough to be further used.

The limiting magnitude of 2.66 is calculated for a 550 km orbit, a framerate of 6/fps and a meteor speed of 40.3 km/s with a radiant angle of 62.55°. The radiant angle is the angle between the nadir direction and the meteor trajectory. The meteor properties are average values determined from the CILBO data base (see [14]).

In order to determine the scientific output, the meteor detection rate must be determined using the calculated limiting magnitude. Therefore, a model giving the number of meteors depending on their brightness is required. Since the brightness depends heavily on the meteoroid mass, mass models are used in a second simulation called *SWARMS Version 2 (SWARMSv2)* [15]. This simulation is based on *Simulator for Wide Area Recording of Meteors from Space (SWARMS)* [16] and has been modified by the Authors.

The simulation takes into account different parameters to determine the number of observable meteors. This includes the limiting magnitude of the instrument as well as the average meteor properties (e. g. velocity, radiant angle) from the CILBO data base, the orbit altitude and the reduction of the apparent meteor brightness due to the meteor movement and the higher distance between observer and meteor.

The working principle is as follows: The number of meteors occurring are determined by using different meteoroid mass models, e. g. the Grün model [17] or the Haliday model [18]. These models give the number of meteoroids above a certain mass occurring per unit of time. Next, each meteoroid is assigned a velocity, travel direction as well as some other properties. Those are used to determine the brightness (magnitude) of the resulting meteor. If the meteor brightness is larger than the minimal brightness required for a successful detection (given by instrument limiting magnitude), the meteor is assumed to be detected. Thus, the detection rate can be determined. The detection rate depends heavily on the used meteoroid model and the meteor properties. This step gives the number of meteors detected by MeSHCam per unit of time. More details about the instrument development and the determination of the detection rates can be found in [19].

### Scientific output depending on satellite bus constrains

Now the number of observed meteors can now be calculated with the detection rates using the actual observation time. This time depends on the resources provided by the satellite bus, mainly the power and data budget but also thermal constrains. For *SOURCE* the following constrains apply: In order to prevent overheating the camera, a maximum operation time of 15 min per observation is allowed. Furthermore, the data budget is limited to 100 MB/day. The energy budget constrains the scientific output significantly, the limitations depends on the orbit type as well as the time between observation. Thus, a separate power simulation developed by the Electrical power supply (EPS) team is used. In order to determine the scientific output a Python script is developed and used to

calculate the generated data and energy demand depending on the total observation time. The total observation time depends on the number of observations, one observation lasts 15 min due to the thermal constrains. In this paper 1 to 5 observations per day are considered.

One observation includes the following steps (also visualized in Figure 9):

1. Orientation of instrument towards nadir
2. Observation of meteors (taking images continuously)
3. Process images (run detection algorithm)
4. Transfer images with meteors to the OBC
5. Downlink images

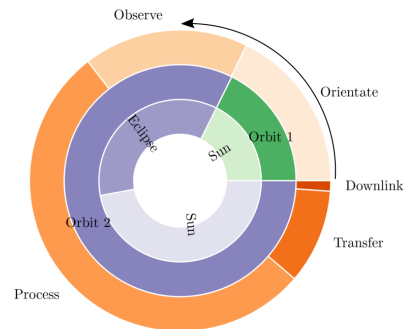


Figure 9. Illustration of the meteor observation concept for *SOURCE* for one 10 min observation.

The Python script calculates the time required for each step depending on the given observation time. Therefore, some assumptions are made, e. g. the time required to orientate the satellite are based on simulations performed by the *SOURCE* team. The processing time depends on the number of images taken during observation and thus on the framerate and observation time. Currently the algorithm required to process the images is taking 0.8 s per image, but a higher processing rate of  $\sim 0.5$  s per images is realistic with future optimizations. Next, the images containing a meteor must be determined, which is done using the meteor detection rate calculated previously. Additionally, a false detection rate of the algorithm of 2 events per hour is assumed based on current tests of the algorithm performance. The total number of images is derived by assuming an event duration and using the framerate of the camera.

Since the images can only be downlinked via the OBC, the images allegedly containing a meteor must be transferred. This is done via a serial interface with a baudrate of 115 200. Measurements using emulated terminals showed that it takes  $\sim 30$  s to transfer one 0.4 MB image.

Finally, the images must be downlinked, the time required is determined with the downlink data rate of the satellite bus and the amount of images and the known image size.

Next, the data budget is considered using the total number of images for downlink to determine if the downlink budget is exceeded.

Finally, the time required for each step together is used to calculate the required energy. Since the camera is only turned on during observation, but the PLOC is required for all other steps except the downlink, the energy budget is calculated separately for PLOC and camera.

The script allows to set different number of observation times and calculates the time, data and energy budget for each given observation time. For time, data and energy budget tables are generated for evaluation.

**Power simulation** Since the available power budget depends on several factors, such as the orbit type and the time between two observations, it is not possible to give a simple power budget for the meteor observation. Instead, the power simulation developed by the EPS team is used. This simulation allows to determine the State of Charge (SoC) of the battery and the power consumption depending on the orbit type and duration of the observation. Thus, in the simulation three steps are simulated (energy consumption stated does not include any margin):

1. Meteor observation (PLOC and MeSHCam) (19.2 W)
2. Processing, image transfer (only PLOC) (15.2 W)
3. Idle mode to charge battery (9.94 W)

These steps are repeated for a set amount of time (24 h). As a result, the SoC and power consumption are plotted over time.

For this analysis a Sun-synchronous Orbit (SSO) is assumed with an altitude of 500 km and a beta angle of  $50^\circ$ . A more detailed analysis of the power budget is possible, once the exact orbit is known. For a rough estimate of the expected scientific output, these assumptions are sufficient. For the determination of the power budget, it is assumed the SoC should not be below 60 %.

### 3.1.2. Results

**Limiting magnitude and detection rates** The meteor detection rates determined with the Grün [17] and Halliday [18] model are shown in Figure 10. As can be seen, the Grün model generates at least one order of magnitude more meteors compared to the Halliday model. This is due to the fact that the sporadic meteoroid flux is not well constrained and due to the data the models are based on: The Halliday model is generated from large meteor events (fireballs) while the Grün model is obtained from in-situ dust measurements as well as from studying lunar micro craters. Thus, the Halliday model is biased for

heavier meteoroids and brighter meteors while the Grün model is more accurate for fainter meteors. Nevertheless,

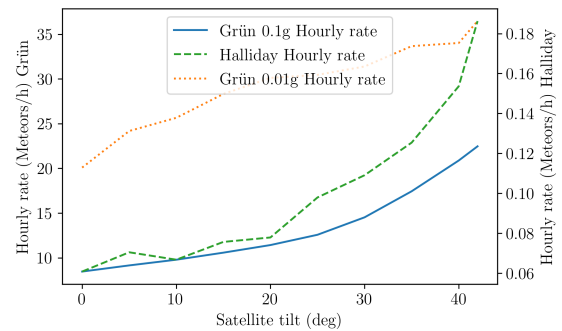


Figure 10. Meteor detection rates of MeSHCam in an orbit, simulated with different meteoroid mass models.

both models are based on actual measurements and can be used to estimate the scientific performance. It has to be kept in mind that the actual measured rate might be different. Due to the larger detection rate, the Grün model is used to determine the images containing a meteor and thus the transfer and downlink time as well as the amount of data to be downlinked. This ensures the worst case is analysed.

The expected scientific output on the other hand is determined with both models as well as the average value in order to get the range of detected meteors during the mission.

Lastly, the SWARMSv2 simulation also allows to set the minimal mass until meteoroids should be generated. For the Grün model two different scenarios are used, one with a minimal mass of 0.01 g and one with 0.1 g. With the lower minimal mass more meteoroids are generated, however these are lightweight and result in fainter meteors. Some of the fainter meteors are observable by the instrument according to the simulation, thus the detection rate increases. However, the meteor might not be detected by the detection algorithm, since fainter meteors are more challenging to detect. Therefore, the higher minimal mass is used for further evaluation.

As can also be seen in Figure 10 as well as Table 4, the detection rate depends on the tilt angle of the satellite. The tilt angle describes the angle between the nadir direction and the optical axis of the instrument. By tilting the satellite, the observed area increases. Since the detection rate depends on the area, a larger observed area increases the detection rate.

For the scientific output and to determine the operation time of the instrument without exceeding any budget, a tilt angle of  $10^\circ$  is assumed.

**Scientific output depending on satellite bus constrains** In Table 5 the time needed for the different steps of the

Table 4. Detection rates (meteors/h) of MeSHCam in an 500 km orbit, simulated with different meteoroid mass models.

Tilt angle (deg)	Grün 0.1g	Halliday	Average
0	8.46	0.06	4.26
5	9.15	0.07	4.61
10	9.79	0.07	4.93
15	10.57	0.08	5.33
20	11.43	0.08	5.75
25	12.57	0.10	6.34
30	14.53	0.11	7.32
35	17.44	0.13	8.78
40	20.88	0.15	10.51
42	22.46	0.19	11.32

Table 5. Time budget for different observation times at 6 fps in a 500 km orbit. The selected option is marked in grey.

	15	30	45	60	75
Observation time total (min)	15	30	45	60	75
Orientation time (min)	15	30	45	60	75
Process time acc. (min)	45	90	135	180	225
Image transfer time (min)	9	17	26	34	43
Downlink time (min)	0.9	1.9	2.8	3.8	4.7
Total time (min)	85	169	254	338	423
Total orbits	0.9	1.9	2.8	3.8	4.7

meteor observation are given for different numbers of observations. See Figure 9 for a visualisation of the process.

A range of 1 to 5 observation each lasting 15 min are evaluated. As can be seen, for one 15 min observation, additional 70 min are required, most of the time dedicated to running the processing algorithm. It is assumed, the satellite needs 15 min for orientation to nadir pointing of the camera. As mentioned above, the processing time is calculated from the framerate, observation time and the processing speed of the algorithm. The total time needed for one observation is later required to calculate the required power.

Next, the data budget must be analysed as shown in Table 6. The data budget is determined using the observation time, framerate and the size of one image. This gives the total amount of images and data generated. The downlink data is determined using the above calculated meteor detection rate and an average meteor duration, to determine the amount of images containing a meteor. Here, the detection performance of the algorithm is also considered. It is assumed, 2 meteors are detected as false positive per hour.

As can be seen, the data to downlink of all observation is well below the available data budget of 100 MB. This means, the data budget is not the limiting factor for the

Table 6. Data budget for different observation times at 6 fps in a 500 km orbit. The selected option is marked in grey.

	15	30	45	60	75
Observation time total (min)	15	30	45	60	75
Data generated (GB)	2.11	4.22	6.33	8.44	10.55
Images generated (k)	5.4	10.8	16.2	21.6	27
Images with meteor	18	35	53	71	88
Data to downlink (MB)	7	14	21	28	35
Detected meteors	2.45	4.89	7.34	9.79	12.24

scientific output of the mission. Since the data budget is not used completely, the detection algorithm can be tuned to detected more false positive but reduce false negatives, in order to not miss any meteor and increase the scientific output.

Finally, the power budget is analysed. The script gives the power to run the PLOC and MeSHCam during the observation as shown in Table 7. As mentioned earlier, the available power budget highly depends on the orbit and an idle phase between observations during which the batteries are recharged.

Table 7. Energy budget for different observation times at 6 fps in a 500 km orbit. The selected option is marked in grey.

	15	30	45	60	75
Observation time total (min)	15	30	45	60	75
Energy consumption PLOC (Wh)	4	8	12	16	20
Energy consumption camera (Wh)	1	2	3	4	5
Energy consumption total (Wh)	5	10	15	20	25

Thus, the power simulation is used in which three simplified steps for meteor observation are considered (see Table 5): 15 min observation with PLOC and MeSHCam turned on followed by 70 min processing, image transfer and orientating of the satellite with only the PLOC turned on. This is a simplified approximation of a meteor observation, but accurate enough to simulate the power budget. Each observation is followed by 250 min of idle mode with sun orientation to recharge the batteries. Thus, in 24 h, 4 complete observations taking 22.3 h are possible.

As can be seen in Figure 11, after the 4 observations the SoC is slightly above the required 60 %. For the scientific output, it is assumed that 4 observations are possible.

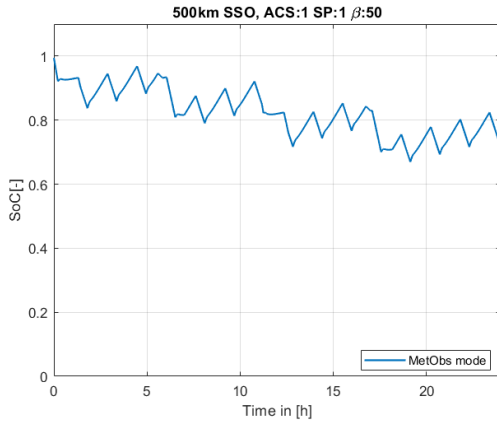


Figure 11. Battery SoC for 4 observation in 24 h in a SSO orbit with a beta angle of  $50^\circ$

In Figure 12 the power consumption is plotted over time. It can be seen, that the power budget is negative, since the mean consumption is above the intake. Therefore, the satellite must recharge the batteries before another set of 4 observation can be started. Thus, not every day of the mission can be used for meteor observation. For the final calculation of the scientific output, it is assumed that 30 % to 50 % (121 d to 182 d) of the 1 year mission can be used for meteor observation.

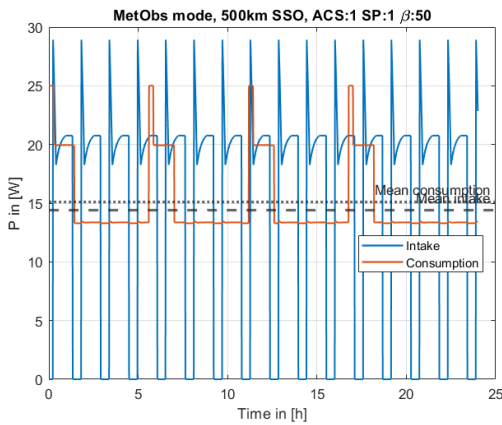


Figure 12. Power consumption and intake for 4 observation in 24 h in a SSO orbit with a beta angle of  $50^\circ$

**Expected output** The number of observable meteors is mainly limited by the power budget and the speed of the detection algorithm. Assuming an average detection rate of  $4.93 \text{ meteors/h}$  (see Table 4) and an observation time of 1 h/d for 121 d to 182 d,  $596 \text{ meteors}$  to  $897 \text{ meteors}$  can be observed during the mission. In the worst case with an detection rate of  $0.07 \text{ meteors/h}$  (Halliday model) and the same observation times,  $8 \text{ meteors}$  to  $13 \text{ meteors}$  can be observed during the mission.

The actual number of detections depends of course on the actual meteor activity as well as on how well the detection algorithm works. Currently, the algorithm is able to detected 78.9 % of all meteors in our current laboratory setup. Assuming this value can be achieved during orbital operation, the number of detected meteors is reduced to  $470 \text{ meteors}$  to  $708 \text{ meteors}$  in the best case and  $6 \text{ meteors}$  to  $10 \text{ meteors}$  using the lowest detection rate.

### 3.2. Current status

Since *SOURCE* is currently in Phase D, testing of the qualification models has been the main focus. This contains hardware test like thermal-vacuum and shaker tests with implemented full functional tests as well as testing and developing PLOC software and the algorithm *SpaceMEDAL*. In the following, the current status of the algorithm *SpaceMEDAL* and its testing software *Artificial Meteorvideo Simulation Software (ArtMESS)* is outlined. Furthermore the tests of MeSHCam hardware and the PLOC software are explained.

#### 3.2.1. Meteor detection algorithm

The meteor detection algorithm *SpaceMEDAL* is used onboard the satellite, but unlike the hardware of a satellite it can be optimized and updated during operation. Nevertheless it is important to test and improve *SpaceMEDAL* before launching *SOURCE*. Therefore, it must work at the testbed in the clean room first. The testbed ( as described in 3.0.3) is an important facility to allow for repeatable and constant testing conditions required for algorithm testing and design. The testbed is used to display test videos imaged by Meshcam in order to generate realistic test data. A large data base of testing material is also needed, which is why *ArtMESS* was developed [20].

*ArtMESS* generates videos showing the Earth at night with simulated meteors. Since MeSHCam is pointing towards the Earth, *ArtMESS* uses monochromatic videos taken from the ISS as well as videos generated from publicly available images showing the Earth at night. *ArtMESS* illustrates a meteor through a moving light sphere with a different direction and velocity as the apparent movement of lights on the Earth caused by satellite movement. This assumption can be made, because the algorithm does not cover the specific case of a meteor moving in the same direction and velocity as the Earth or *SOURCE*. Figure 13 shows an image, which was generated with *ArtMESS*. This testing procedure allows to optimize the algorithm before launch.

**Calibration of testbed** Simulating the view of MeSHCam in orbit on the clean room television requires specific settings and a calibration with MeSHCam. Before testing *SpaceMEDAL* with *ArtMESS* generated videos,

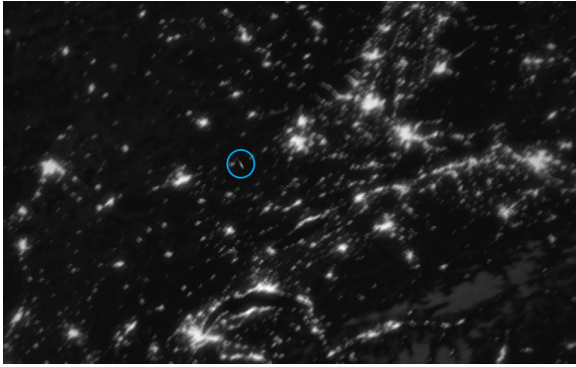


Figure 13. Image of the Earth with a meteor in the blue circle, simulated with ArtMESS

the television was irradiance calibrated. For this calibrations the clean room was darkened and the curtains around the screen were closed to avoid any remaining stray light. While measuring the irradiance with an optometer, five different monochromatic gray images at different brightness and contrast settings of the TV were shown. This procedure has shown that the emitted irradiation level from the TV is too high, compared to a meteor as seen from MeSHCam in space. According to the results the settings of the television were adjusted. Additionally, the aperture of the lens must be further closed.

Accordingly, the aperture of MeSHCam needed to be selected. The established data from the television calibration was used as presets for MeSHCam calibration and the same procedure with variable aperture settings on MeSHCam was conducted. As a result of MeSHCam calibration the fitting apertures for different camera settings were defined. These calibrations ensure that the images are neither over or underexposed and the camera image pixels have the same value as expected from actual meteors. With these settings the testbed setup is finished and *SpaceMEDAL* can be tested with *ArtMESS* generated videos. See [19] for more details on the calibration procedure.

**SpaceMEDAL** The basic idea of the meteor detection algorithm is comparing images and distinguishing meteor movement from background movement [11]. MeSHCam supplies the algorithm with six black and white images per second for up to 15 min. *SpaceMEDAL* compares each image with the following procedure.

The algorithm has to differ between background movement caused by the satellite movement and movement caused by a meteor. In order to differentiate the background from a meteor the algorithm uses the Farneback's dense optical flow calculation [21]. It defines features of interest, e.g. bright pixels as blobs. Multiple blobs moving with a similar velocity and in a similar direction they get defined as the background movement. The blobs from the meteor are left and get detected as a meteor. The images with detected meteors are stored and can be downlinked.

*SpaceMEDAL* is currently able to detect 78.9% of the meteors correctly. This is distinct from a perfect detection rate as each individual background-meteor combination would require a specific parameter set in the algorithm in order to detect every meteor. As it is still getting tested and developed, there will be an improvement of this number until the launch. Even after the launch the parameters can be adjusted, so that the number of detected meteors increase. Thus, the algorithm can be tuned to detect almost all meteors, accepting more false positives or decrease the false positive detections and not detected all meteors. This depends on the available data budget.

### 3.2.2. PLOC software

On *SOURCE* the PLOC is responsible for controlling the cameras and processing the images of MeSHCam with *SpaceMEDAL*. Therefore, the control software for both cameras, the described algorithm for meteor detection, functions to control the operating system as well as the handling of different files need to be implemented. The software operates on Ubuntu and uses the Flight Software Framework (FSFW) developed by the University of Stuttgart's Institute of Space Systems. The latest test of PLOC software has shown that it can communicate with both of the camera systems MeSHCam and PRIMA simultaneously and receive commands from the OBC.

After the test, the focus now is on implementing the algorithm *SpaceMEDAL* and further improving the working camera software. As described in 3.2.1 the algorithm is still being tested and further developed, but it already can be implemented into the payload on-board software. That gives also the opportunity to test updating *SpaceMEDAL* directly on PLOC.

### 3.2.3. Environmental tests

MeSHCam and PLOC are commercial off the shelf components, which are not designed to be used in space. The components need to withstand high and low G-forces, low pressures and large changes in temperature. Therefore, tests are needed to ensure the functionality after launch and in space. The thermal-vacuum test verifies the instruments resistance for temperature and low pressure. The launch is simulated through vibration during the shaker test. It ensures the satellite survives the loads during launch.

**Thermal-vacuum test** In order to ensure that the hardware can withstand the major temperature changes over an eclipse a thermal-vacuum test of MeSHCam was successfully performed. The thermal-vacuum chamber at the University of Stuttgart was used for eight thermal cycles so it complies with the ECSS standard [22]. As described

there, the test contains one non-operating temperature cycle and seven continuous load cycles on a constant pressure level. The focus of the first cycle is on the greatest non-operational temperatures of  $80^{\circ}$  and  $-40^{\circ}$ . The other seven cycles are used to test the long term temperature changes. Several functional tests were successfully performed during the first and last cycle, which confirms the functionality in the operational temperature range. The operational temperature range is specified in the data sheet of MeSHCam [23]. The thermal cycles of MeSHCam test are shown in Figure 14.

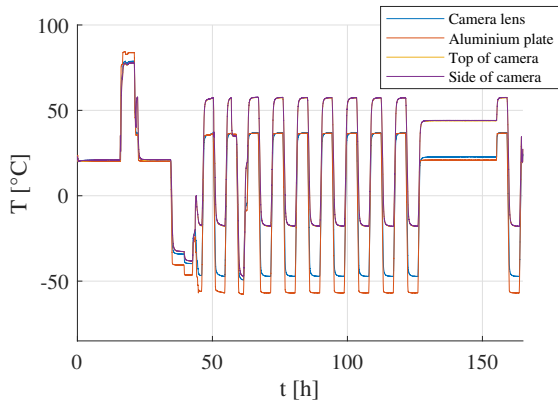


Figure 14. Thermal cycles of the thermal-vacuum test of MeSHCam. The colored lines show the temperature profile of the sensor placed in a specific spot, which is shown in the legend

Before and after the thermal-vacuum test, MeSHCam was tested in the clean room in front of the Ulbricht sphere. By comparing the images from the pre and post test damages on the camera could be excluded. Since the test was a success MeSHCam hardware is able to fulfill its purpose in space.

**Shaker test** The *SOURCE* team is currently preparing for the shaker test of the qualification model of the assembled satellite. This test simulates vibrations, which appear during launch. Therefore, the qualification model of the camera system is installed in the satellite. The placement is shown in the Figure 15. Before and after the shaker test, a full functional test is performed to check the success of the test. Is this test successful, the camera system is able to withstand the upcoming vibration during the launch.

#### 4. SUMMARY AND OUTLOOK

In this paper we presented the scientific mission of the *SOURCE* satellite from University of Stuttgart's Institute of Space Systems and KSat e.V. and outlined the expected scientific output. *SOURCE* is currently in Phase D, after the planned launch 2023/2024 it will be the first mission to combine re-entry measurements of temperature,

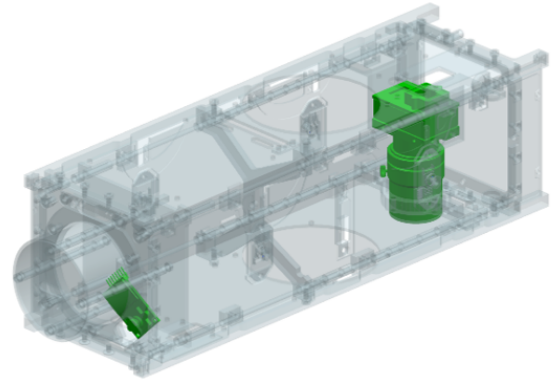


Figure 15. Placement of MeSHCam (right) and PRIma (left) in green in the satellite *SOURCE*

pressure and heatflux to investigate the demise process. Therefore, sensor arrays are developed which combine commercially available sensors and sensors developed at the University of Stuttgart. Additionally, atmospheric science will be conducted by measuring the atomic oxygen concentration using FIPEX sensors developed at the University of Stuttgart.

Furthermore, *SOURCE* will be the first mission dedicated to meteor observation from space and demonstrate the feasibility of space borne meteor detection using onboard image processing for meteor detection. The development and demonstration of the detection algorithm can be used in more complex successor missions and thus contribute to meteor science. Furthermore, the data gathered during the mission will be used to improve existing meteoroid mass models.

All in all, *SOURCE* has a very ambitious scientific mission and shows the feasibility to conduct complex scientific measurements in a small CubeSat developed by students with support from PhD students and researchers.

The hardware for in-situ as well as remote measurements has been developed and tested. The focus is currently on developing the required software and testing the software in an realistic environment such as the Flatsat.

#### ACKNOWLEDGMENTS

The authors acknowledge the high effort and spirit of the *SOURCE* team, who are all doing an amazing job within this project. Furthermore, the authors are grateful for the good support and help of all further involved colleagues at the University of Stuttgart's Institute of Space Systems, particularly the HEFDiG group, the mechanical workshop and the electrical laboratory. We also thank ESA for their support in the *Fly your satellite program!*.

## REFERENCES

- [1] Stefanos Fasoulas et al. “Combining particle-in-cell and direct simulation Monte Carlo for the simulation of reactive plasma flows”. In: *Physics of Fluids* 31 (July 2019), p. 072006. DOI: 10 . 1063/1.5097638 (cit. on p. 2).
- [2] ”Thaddeus Cesari”. *NASA JWST Blog*. {<https://blogs.nasa.gov/webb/2022/06/08/webb-engineered-to-endure-micrometeoroid-impacts/>}. Accessed: 10.06.2022. 2022 (cit. on p. 3).
- [3] Daniel Galla et al. “The Detailed Design of the SOURCE Satellite for Demise Investigation”. In: May 2022 (cit. on p. 3).
- [4] Daniel Galla et al. “IN-SITU MEASUREMENTS IN EARLY PHASE RE-ENTRY OF THE SOURCE CUBESAT FOR NUMERICAL SIMULATION VALIDATION”. In: June 2022 (cit. on p. 3).
- [5] M. Eberhart et al. “Measurement of atomic oxygen in the middle atmosphere using solid electrolyte sensors and catalytic probes”. In: *Atmospheric Measurement Techniques* 8.9 (2015), pp. 3701–3714. DOI: 10 . 5194/amt-8-3701-2015. URL: <https://amt.copernicus.org/articles/8/3701/2015/> (cit. on p. 4).
- [6] Hendrik Kuhm et al. “Design and development of the re-entry sensor system for the CubeSat mission SOURCE”. In: Apr. 2022. DOI: 10 . 5821/conference-9788419184405.103 (cit. on p. 4).
- [7] B. Strelnikov et al. “Simultaneous in Situ Measurements of Small-Scale Structures in Neutral, Plasma, and Atomic Oxygen Densities during the WADIS Sounding Rocket Project”. In: *Atmospheric Chemistry and Physics* 19.17 (2019), pp. 11443–11460. DOI: 10 . 5194/acp-19-11443-2019 (cit. on p. 4).
- [8] M. Grygalashvyly et al. “Atmospheric Band Fitting Coefficients Derived from a Self-Consistent Rocket-Borne Experiment”. In: *Atmospheric Chemistry and Physics* 19.2 (2019), pp. 1207–1220. DOI: 10 . 5194/acp-19-1207-2019 (cit. on p. 4).
- [9] M. Eberhart et al. “Transient Response of Amperometric Solid Electrolyte Oxygen Sensors under High Vacuum”. In: *Sensors and Actuators B: Chemical* 323 (2020), p. 128639. DOI: 10 . 1016/j.snb.2020.128639 (cit. on p. 5).
- [10] M. Eberhart et al. “Atomic oxygen number densities in the mesosphere-lower thermosphere region measured by solid electrolyte sensors on WADIS-2”. In: *Atmospheric Measurement Techniques* 12.4 (2019), pp. 2445–2461. DOI: 10 . 5194/amt-12-2445-2019 (cit. on p. 5).
- [11] Jona Petri, Julia Zink, and Sabine Klinkner. “Hardware accelerated onboard image processing for space-based meteor observation - Concept and Implementation of SpaceMEDAL”. In: Vilamoura, Portugal, 2022 (cit. on pp. 6, 12).
- [12] Marcel Liegibel et al. “Meteor observation with the SOURCE CubeSat – Developing a simulation to test on-board meteor detection algorithms”. In: Barcelona, Spain, 2022 (cit. on p. 7).
- [13] Jona Petri et al. “Design and test of a COTS based imaging system for stereoscopic meteor observations”. In: *Proceedings of IAA Smallsat conference*. 2019 (cit. on p. 7).
- [14] Detlef Koschny et al. “A double-station meteor camera set-up in the Canary Islands – CILBO”. In: *Geoscientific Instrumentation, Methods and Data Systems* 2 (Dec. 2013). DOI: 10 . 5194/gi-2-339-2013 (cit. on p. 8).
- [15] Jona Petri, Julia Zink, and Sabine Klinkner. “Optimizing the scientific output of satellite formation for a stereoscopic meteor observation”. In: *International Meteor Conference Bollmannsruh, Germany*. 2019 (cit. on p. 8).
- [16] Alexis Bouquet et al. “Simulation of the capabilities of an orbiter for monitoring the entry of interplanetary matter into the terrestrial atmosphere”. In: *Planetary and Space Science* 103 (2014), pp. 238–249. URL: <https://doi.org/10.1016/j.pss.2014.09.001> (cit. on p. 8).
- [17] E Grün et al. “Collisional balance of the meteoritic complex”. In: *Icarus* 62.2 (1985), pp. 244–272 (cit. on pp. 8, 9).
- [18] Ian Halliday, Arthur A Griffin, and Alan T Blackwell. “Detailed data for 259 fireballs from the Canadian camera network and inferences concerning the influx of large meteoroids”. In: *Meteoritics & Planetary Science* 31.2 (1996), pp. 185–217 (cit. on pp. 8, 9).
- [19] Jona Petri. “Satellite formation and instrument design for autonomous meteor detection”. 1 Online-Ressource (XXVIII, 314 Seiten). Hochschulschrift. Stuttgart, 2022. DOI: 10 . 18419/opus-12568 (cit. on pp. 8, 12).
- [20] Marcel Liegible et al. “Meteor observation with the SOURCE CubeSat - Developing a simulation to test on-board meteor detection algorithms”. In: *Proceedings of SSEA conference*. 2022 (cit. on p. 11).
- [21] Gunnar Farneböck. “Two-Frame Motion Estimation Based on Polynomial Expansion”. In: *Proceedings of the 13th Scandinavian Conference on Image Analysis NCS 2749* (June 2003), pp. 363–37 (cit. on p. 12).
- [22] ESA - ESTEC. “Thermal testing for the evaluation of space materials, processes, mechanical parts and assemblies”. In: *European Cooperation for Space Standardization (ECSS) - Space product assurance* (2008) (cit. on p. 12).

[23] TELEDYNE Dalsa. *Genie™ Nano-M1920* (cit. on p. 13).